communications physics

ARTICLE

https://doi.org/10.1038/s42005-022-01009-8

OPE



1

Bloch oscillations and matter-wave localization of a dipolar quantum gas in a one-dimensional lattice

Gabriele Natale ^{1,2}, Thomas Bland ², Simon Gschwendtner², Louis Lafforgue², Daniel S. Grün², Alexander Patscheider², Manfred J. Mark ^{1,2} & Francesca Ferlaino ^{1,2}

Three-dimensional quantum gases of strongly dipolar atoms can undergo a crossover from a dilute gas to a dense macrodroplet, stabilized by quantum fluctuations. Adding a one-dimensional optical lattice creates a platform where quantum fluctuations are still unexplored, and a rich variety of phases may be observable. We employ Bloch oscillations as an interferometric tool to assess the role quantum fluctuations play in an array of quasi-two-dimensional Bose-Einstein condensates. Long-lived oscillations are observed when the chemical potential is balanced between sites, in a region where a macrodroplet is extended over several lattice sites. Further, we observe a transition to a state that is localized to a single lattice plane-driven purely by interactions-marked by the disappearance of the interference pattern in the momentum distribution. To describe our observations, we develop a discrete one-dimensional extended Gross-Pitaevskii theory, including quantum fluctuations and a variational approach for the on-site wavefunction. This model is in quantitative agreement with the experiment, revealing the existence of single and multisite macrodroplets, and signatures of a two-dimensional bright soliton.

¹ Institut für Quantenoptik und Quanteninformation, Österreichische Akademie der Wissenschaften, Technikerstraße 21a, 6020 Innsbruck, Austria. ² Institut für Experimentalphysik, Universität Innsbruck, Technikerstraße 25, 6020 Innsbruck, Austria. [™]email: francesca.ferlaino@uibk.ac.at

he dipole-dipole interaction (DDI) between magnetic atoms in an ultracold quantum gas has been key to the discovery of supersolids 1-3 and macrodroplets 4,5, states of matter with extremely intriguing and counter-intuitive properties^{6,7}. Macrodroplets are macroscopic quantum states that behave in many ways like liquid droplets^{4,5,8,9}. They are at least an order of magnitude denser than normal Bose-Einstein condensates (BECs), and can be self-bound. They exist in a parameter regime in which mean-field theories predict the collapse of the entire system when the attractive dipolar interactions overcome the repulsive contact interactions. Instead, the system remains stable thanks to the so-called quantum fluctuations, thus providing one of the rare examples where beyond-mean-field interactions substantially change the ground state of the system^{10,11}. Although the functional form of the beyond-meanfield term, otherwise known as the Lee-Huang-Yang (LHY) correction¹², is still subject to intense study and debate^{13,14}, its importance is now undoubted. Isolating beyond-mean-field effects may be crucial to settle disputes on its validity, particularly in dipole dominated systems; however, it is very difficult to have access to individual interaction contributions. Though, the differing atom number scaling between mean-field and LHY contributions provide a promising method to differentiate between them.

Optical lattices enable powerful interferometric approaches to, e.g., measure with high precision the zero-crossing of the scattering length or of the mean-field interaction with the so-called Bloch oscillation (BO) technique^{15–18}, and to achieve an accurate determination of the background scattering length via lattice spectroscopy in Hubbard models^{4,19,20}. Moreover, the presence of the lattice itself may change completely the phase diagram of the system, as shown in seminal experiments with contact interacting gases^{21–23}. Unique phenomena are predicted with the addition of long-range DDIs^{24,25}. Experiments with lattice-confined atomic dipolar gases have already shown important results, e.g., the realization of extended Bose-Hubbard models²⁶ and spin models²⁷⁻³⁰ in three-dimensional (3D) lattices. In 2D lattices, forming quasi-1D tubes, suppression of dipolar relaxation³¹ and the controlled breakdown of integrability³² have been observed. Instead, up to now, 1D lattices, forming an array of quasi-2D layers, have been used with large wavelengths to load a single pancake trap³³, or multi-layer traps to study the role of DDI in the stability against collapse 34. Further, theoretical proposals have suggested that the DDI between layers not only can lead to modifications within each layer^{35–38} but also to inter-layer bound states^{39–41}. Other works predict the existence of bright-soliton structures along the lattice⁴² or anisotropic on-site solitons^{43,44}. However, those proposals lack the important stabilization mechanism given by the LHY term, which is known to provide many intriguing phases in continuous systems (e.g., harmonically trapped), opening up many questions: What is the ground state of an attractive dipolar gas in a 1D lattice potential? Can droplets be delocalized over many lattice planes? Will solitonic solutions continue to exist?

In the present work, we study an erbium dipolar gas in a 1D optical lattice with dominantly attractive DDI. We employ BOs as an interferometric tool to probe the interaction contributions of the system, and to isolate the role of beyond-mean-field effects. We find long-lived oscillations, associated with a minimum in the dephasing rate, close to the cancellation point between mean-field and beyond-mean-field interactions, and at scattering lengths significantly shifted from the expected mean-field result. We develop a discrete effective 1D extended Gross-Pitaevskii equation (eGPE) with variational transverse widths 45,46. We find that this minimum occurs when the chemical potentials on each site are equal, not the energies—as has been employed successfully in

contact interaction dominated systems ^{17,18}—due to the difference in density scaling between the interactions. The close correspondence between theory and experiment shows the validity of the LHY prediction, even while highly inhomogeneous densities are expected to break the local density approximation¹². Moreover, we see that for low scattering lengths the system undergoes a structural transition to a single localized 2D plane, signifying an interaction-driven approach to generate systems in reduced geometries. Finally, using our theoretical model we produce a full phase diagram of the system, revealing the impact of the LHY contribution to the predicted 2D anisotropic soliton state⁴³, which is instead morphed into a droplet solution at high atom numbers. Though, promisingly, we still find soliton-like solutions exist.

Results and discussion

Setup and preparation. In the experiment, we prepare a degenerate dipolar gas of erbium atoms in a one-dimensional optical lattice as follows. We start with a dipolar quantum gas of 5×10^4 spin-polarized ^{166}Er atoms confined in a cigar-shaped optical dipole trap 47 elongated along y. Typical BEC fractions range from 60% to 80%. The dipolar length for ^{166}Er is fixed at $a_{\text{dd}} = 66.5 \ a_0$, where a_0 is the Bohr radius. We change the contact interaction between atoms and therefore the s-wave scattering length a_s , via Feshbach tuning 48 using a resonance located near zero magnetic field 20 , as detailed in the "Methods" section. We fix the orientation of $\bf B$ to be along the weak axis (y) of the trap, making the DDI dominantly attractive 4,7 .

Once the harmonically trapped cloud is prepared at the desired a_s , we switch on a 1D optical lattice, aligned along the gravity direction (z); see Fig. 1(a). The vertical lattice is created by retroreflecting a $\lambda=1064$ nm laser beam. We load the planes by exponentially increasing the lattice depth V_0 to $8\,E_{\rm rec}$ in 20 ms, where $E_{\rm rec}=\hbar^2k^2/2m=h\times10.5$ kHz. Here, $\hbar=h/2\pi$ is the reduced Planck's constant (h), m is the mass of $^{166}{\rm Er}$ atoms and $k=2\pi/\lambda$ is the wave-vector of the lattice. The 1D lattice forms an array of tightly confined quasi-2D planes with a trap frequency along the tight direction $\omega_z\simeq 2\pi\times 6$ kHz, corresponding to an harmonic oscillator length $z_{\rm ho}=100$ nm. Due to the transversal Gaussian profile of the lattice beam, we estimate a residual trap of frequencies $\omega_{x,y}=2\pi\times (4,4)$) Hz. The tunneling rate, J, between planes is about $h\times 33$ Hz. For these 1D lattice parameters, $\hbar\omega_z>k_BT$ and the system is kinematically $2D^{49}$.

Bloch oscillations in a one-dimensional optical lattice. We first aim at inducing Bloch oscillations to interferometrically assess the role of beyond-mean-field effects and test the validity of the LHY term. We thus suddenly switch off the dipole trap and let the system evolve in the combined lattice and gravitational potential for a variable hold time $t_{\rm h}$. Finally, using standard absorption imaging after 30 ms of time-of-flight (TOF), we record the evolution of the momentum distribution and extract the position of the main peak, $q_{\rm max}$, as a function of $t_{\rm h}$. Figure 1b shows an exemplary set of absorption images during a single Bloch period $T_{\rm BO}$. We observe the key paradigm of BOs, i.e., the linear increase of the mean momentum due to the acceleration and the Bragg reflection occurring at the border of the Brillouin zone⁵⁰, well described by fitting a sawtooth function to $q_{\rm max}$.

described by fitting a sawtooth function to $q_{\rm max}$. The high sensitivity of BOs to interactions 17,51 clearly appears by tracing the evolution for two different $a_{\rm s}$ (see Fig. 1c, d), as the interaction dependence is encoded into the dephasing rate. For a contact-dominated gas ($a_{\rm dd} < a_{\rm s} = 90~a_0$, Fig. 1c), we see that the BOs vanish within a few $T_{\rm BO}$. On the contrary, decreasing $a_{\rm s}$, and thereby going into the regime where contact interactions and DDI nearly compensate each other ($a_{\rm s} = 60~a_0$, Fig. 1d), we observe

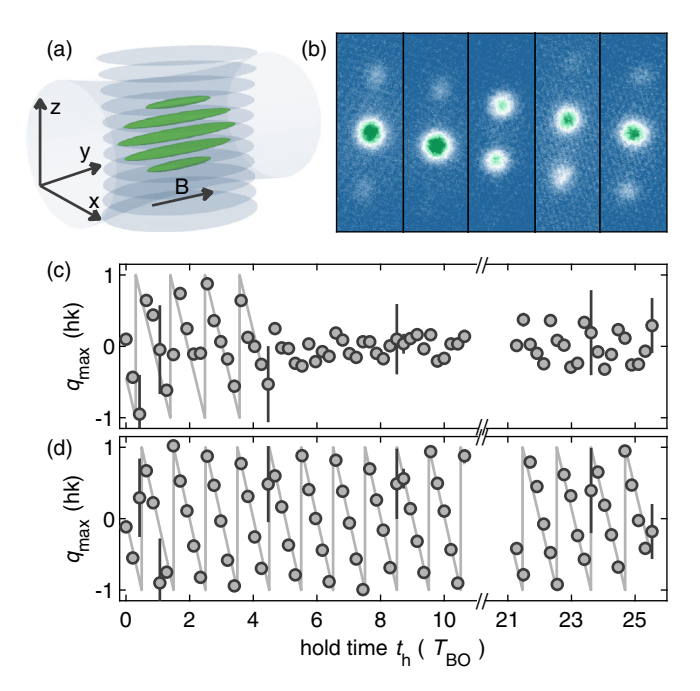


Fig. 1 Bloch oscillations of a dipolar BEC in a one-dimensional optical lattice. a Sketch of our experiment, consisting of a 1D optical lattice in the *z*-direction, loaded with an erbium BEC from an optical dipole trap with trapping frequencies $\omega_{x,y,z} = 2\pi \times (240(3), 30(3), 217(1))$ Hz. Gravity acts along *z*. **b** Absorption images after time of flight (TOF) showing the momentum distributions during one Bloch cycle. **c**, **d** Evolution of the peak position of the momentum distribution (a_{max}) for $a_s = (71.6(1.0), 59.8(1.0))$ a_0 , respectively. A sawtooth fit (solid gray) to the data yields $T_{BO} = 0.469(4)$ ms, consistent with the expected value $T_{BO} = 2k/(mg_{grav})$. The error bars represent the standard error on the mean over 4–6 repetitions.

persisting oscillations for more than 25 Bloch cycles, set by our limited observation time (for details on the analysis of the momentum distribution during Bloch Oscillation, see Supplementary Note 4). To systematically study this effect, we repeat the BO measurements for different values of $a_{\rm s}$, and extract the corresponding dephasing rate γ . As shown in Fig. 2a, we observe a resonant-type behavior with γ showing a pronounced dip with a minimum at $a_{\rm s}=61~a_{\rm o}$. This minimum is clearly different to the point $a_{\rm s}\approx a_{\rm dd}$, where the variance of the mean-field energies across different lattice sites cancel 18, which would be expected from previous observations 17,51.

To get further insight on the origin of the minimum, we develop a discrete effective 1D eGPE, inspired by the close correspondence between predictions from discrete models and experimental observations in non-dipolar^{52,53} and weakly dipolar¹⁸ BECs. We separate the 3D wavefunction into radial and axial contributions, allowing for a variational anisotropic radial width and thus maintaining the 3D character⁴⁵. Along the lattice direction (z), we further decompose the wavefunction, $\psi(z,t)$, as a sum of Wannier functions w(z) of the lowest energy band over all lattice sites: $\psi(z,t) = \sqrt{N \sum_i c_i(t) w(z-z_i)}$, where N is the atom number and $c_i(t)$ the complex wavefunction amplitude on lattice site j, leading to a set of discrete effective 1D eGPEs, each including mean-field and beyond mean-field interactions. For the beyond-mean-field interaction, the 3D form of the LHY still fully applies since the contact interaction energy exceed the confinement energy scale (for details on the 2D to 3D crossover, see Supplementary Note 2)⁵⁴. However, our system may also open to further studies on the 2D to 3D crossover of the LHY. We solve these equations coupled to a minimization of the

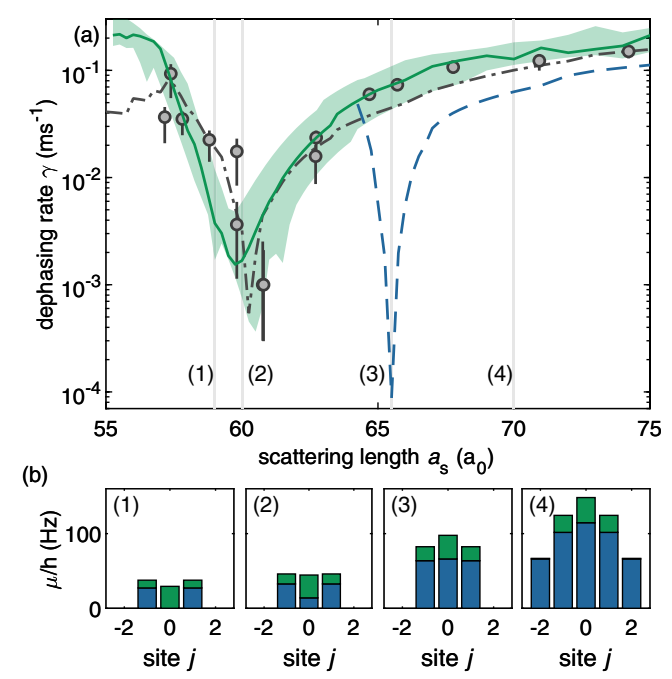


Fig. 2 Dephasing rate and chemical potential distributions. a Experimental dephasing rate γ (circles) as a function of scattering length $a_{\rm s}$. The green solid line shows the theory result, with an uncertainty region (shaded area) accounting for 20% atom number variation. The blue dashed line shows the theory expectation without Lee-Huang-Yang (LHY). The gray dot-dashed line gives the prediction of the semi-analytic approximation for γ . Error bars show the 68% confidence interval (see Supplementary Note 4 for details on the analysis of the momentum distribution during Bloch Oscillation). The statistical uncertainties on the scattering length is smaller than the symbols size. **b** Chemical potential per lattice site μ_j extracted from the discrete model for $a_{\rm s} = (59, 60, 65.5, 70)$ $a_{\rm O}(1, 2, 3, 4)$. The green area depicts the LHY contribution to μ_i .

energy functional with respect to the variational parameters to determine the ground states, benchmarking them against the full 3D theory. We then perform dynamic simulations of the expected time evolution (see the "Methods" section), giving an accurate dephasing rate (solid line) in Fig. 2a without free parameters.

In previous studies^{17,18}, the point of minimum dephasing was found to occur when the mean-field interaction energies vanish or cancel. We isolate the mean-field contribution by removing beyondmean-field effects from our simulations (dashed line in Fig. 2a), predicting a minimum at $a_s \approx a_{dd}$. However, this is in clear contradiction with our experimental observations by a shift of 6a₀ and a different overall shape due to the different scaling of the LHY term with the density. Without LHY, the cancellation of mean-field energies, E'_{MF} , is equivalent to the cancellation of onsite chemical potentials, given by $\mu_j = 2E_{\rm MF}^j/|c_j|^2$. Note, μ_j dictates the wavefunction phase winding on each site through $c_i = |c_i|e^{-i\mu_jt/\hbar}$. Reintroducing quantum fluctuations, we obtain $\mu_j = (2E_{\rm MF}^j + 5/2E_{\rm BMF}^j)/|c_i|^2,$ where the 5/2 appears due to the $|c_i|^5$ density scaling in the beyondmean-field energy (E'_{BMF}). Figure 2b shows μ_i from the ground state calculation for four scattering lengths, additionally indicating the contribution of the LHY correction.

We observe that the point of minimal dephasing in the experiment is close to the point where the variance of μ_j is minimized. Indeed, within a semi-analytic approximation (see Supplementary Note 3 for details on the analytic model of dephasing), we find a direct relationship between γ and μ_j , which reads $\gamma \propto |\mu_1 - \mu_0|$ when 3 lattice sites (j = -1, 0, 1) are occupied.

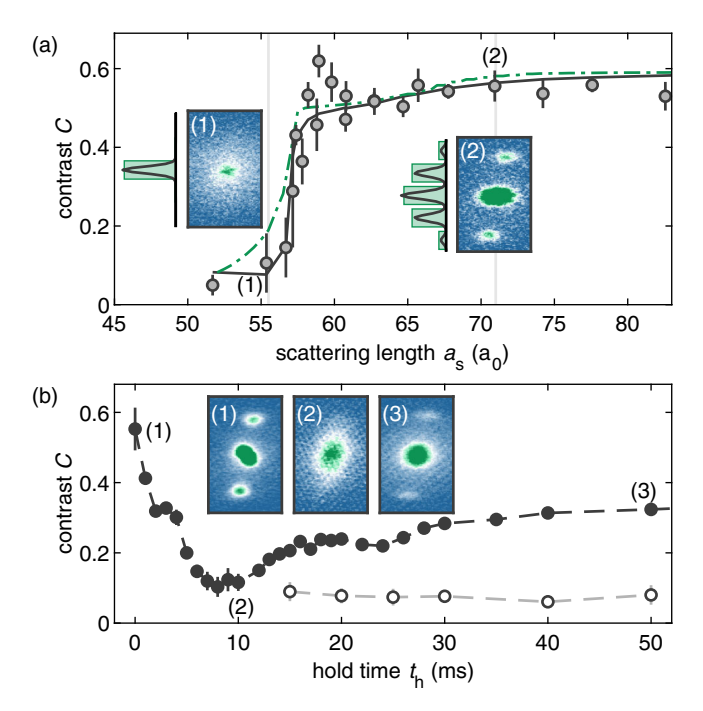


Fig. 3 Interaction-induced localization. a Contrast of the interference pattern after loading the lattice at different $a_{\rm s}$. The green dot-dashed (black solid) line represents the result of the 1D discrete model (3D extended Gross-Pitaevskii equation, eGPE) multiplied by 0.7. The insets show the respective density distributions along z of the 1D discrete model (bars) and 3D eGPE (lines) and corresponding experimental averaged interference patterns after TOF expansion (1,2). The statistical uncertainties on the scattering length is smaller than the symbols size. **b** Dynamic evolution of the contrast quenching back (filled circles) or holding $a_{\rm s}$ (open circles); see text. The error bars represent the standard error on the mean over 4–6 repetitions.

This model can be extended to 5 lattice sites, giving the dot-dashed line (Fig. 2a) which reproduces very well the system behavior. These results lead us to believe that measuring the dephasing rate through the chemical potential will be ubiquitous to systems with arbitrary interaction potentials, which can be substantiated through future work. Note, the total (MF + LHY) interaction energies over the system cancel at $57.5 \, a_0$, which does not coincide with the minimum of the dephasing, occurring at approximately $60 \, a_0$. Additionally, we mainly attribute the asymmetric shape of the dephasing rate in both the theory and experiment to the change of the number of occupied sites in the ground state, which smoothly reduces from ~5 to 3 from 75 to $60 \, a_0$, before rapidly reducing to a single occupied lattice site at ~55 a_0 (see later discussion and insets of (Fig. 3a).

Interaction-induced single site localization. By decreasing the scattering length below 57 a_0 , no BOs nor interference peaks are visible anymore. We observe at the initial instant ($t_h=0$ ms) that the momentum distribution is already spread over the entire first Brillouin zone. To quantify this, we study the contrast, C, of the interference pattern of the initial momentum distribution as a function of a_s , see Fig. 3a. We extract C, defined as the amplitude of the momentum peaks at $\pm 2\hbar k$ relative to the zero momentum peak, from the Fourier analysis of the TOF images (see the "Methods" section). For large a_s , we observe the typical matterwave interference pattern, as expected from a coherent state populating several lattice planes (see inset)⁵³. As we lower a_s , C first remains fairly constant. For a_s below a certain critical value $a_s^* \approx 57 \, a_0$, we observe a sudden loss of the interference pattern with a sharp decrease of C to almost zero.

Additionally, we observe that this interaction-driven process is reversible. To test the restoring of the interference pattern, we employ the following protocol (see the "Methods" section): In brief, we first prepare the system in the lattice at constant and large a_s ($a_s = 69(2) a_0$). We then ramp down a_s below a_s^* $(a_s = 56(2) a_0)$ in 20 ms and wait until C stabilizes to a small value; see Fig. 3b. Note that the interference pattern disappears after about 10 ms, which is on the order of the tunneling time h/Ibetween two neighboring lattice sites. At this point, we quench a_s back to its initial value and probe the time evolution of the system towards its new equilibrium state. On a similar timescale, we observe the reappearance of the interference pattern with an increase of C, which then saturates to about 60% of its initial value. We attribute the partial recovery of the contrast to an increase of the losses and heating. These arise from the combined effect of an increase of the density and three-body scattering rates occurring when tuning the magnetic field closer to a Feshbach resonance⁴. For comparison, we also show the data without inverting the field ramp.

The observed broad distribution in reciprocal space suggests that the system ground state has undergone a structural change, with the macroscopic wavefunction localized in one lattice plane. To verify this interpretation, we calculate the ground state of the system as a function of a_s . When the repulsive contact interaction dominates $(a_s > a_{dd})$, we find an array of BECs occupying approximately three to five lattice planes; see insets Fig. 3a. In contrast, when the relative strength of the attractive dipolar interaction with respect to the other terms in the Hamiltonian is increased, the system reaches a critical point. Here, it undergoes a phase transition to a quasi-2D state, in which all atoms are localized into a single lattice plane to minimize their energy. This purely interaction-driven phase transition-somewhat reminiscent of a continuous version of a superfluid to Mott insulator transition⁵⁵-is stabilized by quantum fluctuations (LHY), preventing the subsequent collapse of the system^{42,56}. The predicted critical point occurs exactly where we observe the disappearance of the interference pattern in the experiments. We find an overall excellent agreement between the measured and the calculated C from both the discrete 1D model and the 3D theory without any free fitting parameters, except for a rescaling factor to the contrast amplitude to account for the thermal atoms in the experiment.

Two-dimensional bound states: solitons and droplets. The observation of this phase transition to a quasi-2D localized state driven by interactions points to the existence of a rich variety of phases. The importance of the LHY correction and its peculiar density scaling motivate us to investigate the properties of the ground state as a function of a_s and atom number to identify distinct phases in this unique setting. For this, we employ our discrete model to derive a full phase diagram; see Fig. 4a. To investigate the boundness of the states, we assess the impact of the radial harmonic trap on the minimum of the variational energy, which is a function of the radial widths l_x and l_y (the individual energy contributions are shown in Supplementary Note 1). At large scattering lengths, as expected, we find a stable delocalized BEC phase, where the total interaction energy (mean-field + LHY) is positive. The state is trap-bound, meaning that there is no energy minimum without the radial harmonic confinement; inset of Fig. 4a.

Reducing a_s , we find an energy minimum even without the radial harmonic trap (Fig. 4b, c), highlighted as colored region in the phase diagram. These quasi-2D self-bound solutions (the lattice still provides axial confinement) are either extended over several sites (lighter color) or localized to a single plane (darker color). In the literature, there are two paradigmatic examples of

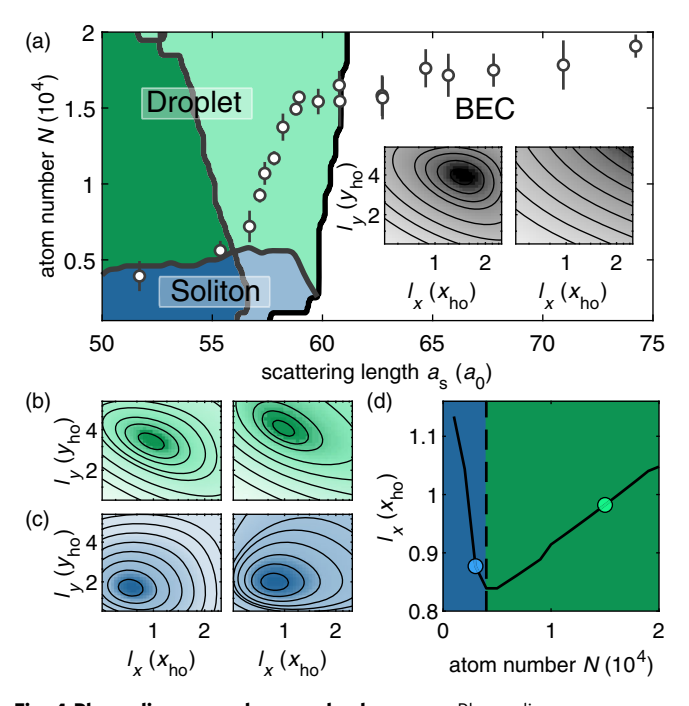


Fig. 4 Phase diagram and energy landscapes. a Phase diagram as a function of a_s and atom number. The white region denotes a trap-bound BEC extended over several lattice sites. The colored regions denote quasi-2D self-bound solutions: a droplet (green), a soliton (blue), each either extended over several lattice sites (lighter shade) or localized (darker shade, >95% of the atoms are localized in the central lattice plane). Circles show the atom number from our experimental data points in Fig. 3a. The statistical uncertainties on the scattering length is smaller than the symbols size. **a-c** Energy landscapes as a function of the radial widths I_x and I_y , in units of the radial harmonic oscillator lengths $x_{ho} = 0.50(1) \, \mu m$ and $y_{ho} = 1.42(1) \,\mu\text{m}$, respectively, with (left) and without (right) the radial harmonic trap, for (a) BEC $(a_s, N) = (70 a_0, 1.5 \times 10^4)$, (b) droplet $(a_s, N) = (65 a_0, 1.5 \times 10^4)$ and (c) soliton $(a_s, N) = (51.5 a_0, 0.4 \times 10^4)$ regimes, with darker shading at the minima. **d** Radial width I_x versus N for $a_s = 51.5 a_0$. The dashed line indicates the soliton-to-droplet transition point, and the circles indicate the position of b, c.

self-bound objects with attractive mean-field energy: droplets and solitons. Droplets can exist in one, two or three dimensions and are stabilized through the LHY correction⁷. Stable bright solitons only exist in quasi-1D systems with attractive contact interactions and are stabilized against collapse purely by kinetic energy. In the search for solitons in higher dimensions, theoretical studies have suggested that the DDI could stabilize such 2D solutions^{43,44}. To the best of our knowledge, there have been no studies on the effect the LHY correction has on this prediction, nor experimental observation. In the present case, where many interactions and kinetic energy compete, a classification of self-bound solutions is much less straightforward. As a crucial distinction between a droplet (Fig. 4b) and a soliton (Fig. 4c), we extract the width l_x from the energy landscape minimum in the radially untrapped system, and investigate its scaling with atom number (Fig. 4d). The soliton width (along the collapse direction) scales inversely with increasing atom number⁵⁷, while in contrast, the droplet size increases in all directions with N^{58} , as predicted in a quasi-1D setting⁵⁹. We use this distinction to draw a boundary between the two phases, observing a phase transition at around 5000 atoms, for both single-site and multi-site solitons. The overlaying of our measurements (Fig. 3a) onto the phase diagram suggests that the experiments have already reached the unexplored regimes of both 2D self-bound droplet and dipolar

solitons. This opens the door to future experimental investigation on the self-bound nature and properties of these 2D phases.

In conclusion, we theoretically and experimentally investigate the behavior of a strongly dipolar quantum gas in a 1D optical lattice. We employ BOs and characterize their dephasing rate as a function of a_s . We observe a minimum in the dephasing shifted $6 a_0$ away from the purely mean-field prediction, providing an interferometric measure of the beyond-mean-field contribution. For low enough a_s , the system enters into a quasi-2D state which is localized onto a single lattice plane, providing a genuine interaction-driven path to reach reduced dimensions in dipolar gases. Using our developed discrete theory model, we derive a full phase diagram which confirms the observed localization transition. This also reveals signatures of quasi-2D self-bound dipolar droplet solutions, and the long sought-after 2D anisotropic dipolar soliton, first predicted in ref. 43 (see also^{44,60}). Our work paves the way for future studies of the soliton-to-droplet crossover in a dipolar gas, as observed in a Bose-Bose gas⁶¹, and of the "solitonic" nature⁶² of dipolar solitary waves^{63–67}. A future promising prospect will be to observe the density profiles with in-situ imaging such to experimentally discriminate between the soliton/droplet regimes.

Methods

Theoretical model. In this work, we use an extended Gross-Pitaevskii theory for direct comparison to our experimental results. We employ both the standard three-dimensional form of the extended Gross-Pitaevskii equation (eGPE) and derive a discrete effective one-dimensional eGPE. Starting with the three-dimensional case, our system can be described by the 3D eGPE of the form^{4,68-70}

$$\begin{split} i\hbar\frac{\partial}{\partial t}\Psi(\overrightarrow{x},t) = & \left[-\frac{\hbar^2}{2m}\nabla^2 + V_{\text{harm}}(\overrightarrow{x}) \right. \\ & + V_{\text{latt}}(z) - F_{\text{ext}}z + g|\Psi(\overrightarrow{x},t)|^2 \\ & + \int d^3\overrightarrow{x}' U_{\text{dd}}(\overrightarrow{x}-\overrightarrow{x}')|\Psi(\overrightarrow{x}',t)|^2 \\ & + \gamma_{\text{QF}}|\Psi(\overrightarrow{x},t)|^3 \right]\Psi(\overrightarrow{x},t), \end{split} \tag{1}$$

where the wavefunction Ψ is normalized to the total atom number $N=\int \mathrm{d}^3 \overrightarrow{x} \ |\Psi|^2$. The atoms are confined in a harmonic potential $V_{\mathrm{harm}}=\sum_{\xi=x,y,z}\frac{1}{2}m\omega_\xi^2\xi^2$ with single particle mass m and trap frequencies ω_ξ , together with the lattice potential $V_{\mathrm{latt}}=sE_{\mathrm{rec}}\sin^2(kz)$ where s is the tunable lattice depth in multiples of the recoil energy E_{rec} and $k=2\pi l \lambda$ is the lattice spacing in reciprocal space. The mean-field interaction contributions are $g=4\pi \hbar^2 a_s/m$ for the contact interaction, governed by the s-wave scattering length a_s , and the long-ranged anisotropic dipolar interaction potential $U_{\mathrm{dd}}(\overrightarrow{x})=3\hbar^2 a_{\mathrm{dd}}/m(1-3\cos^2\theta)/|\overrightarrow{x}|^3$, where $a_{\mathrm{dd}}=\mu_0\mu_m^2m/12\pi\hbar^2$ with magnetic moment μ_m and θ is the angle between the polarization axis (y-axis) and the vector between neighboring atoms. We also include beyond-mean-field effects through the quantum fluctuations term

 $\gamma_{\rm QF}=rac{32}{3}\,g\,\sqrt{rac{a_{
m d}^2}{\pi}}(1+rac{3}{2}\,arepsilon_{
m dd}^2)^{12},$ which depends on the relative strength between the dipolar and short-ranged interactions $\varepsilon_{
m dd}=a_{
m dd}/a_{
m s}$. Finally, $F_{
m ext}=g_{
m grav}m$ denotes the external force exerted on the system by gravity.

In this work, we employ the imaginary time-evolution technique on Eq. (1) in order to find stationary solutions for the wavefunction in the lattice, without gravity. For various atom numbers and scattering lengths, we use a numerical grid of lengths $(L_\infty, L_y, L_z) = (6, 33.3, 6) \mu m$, with corresponding grid points $128 \times 256 \times 128$. The dipolar term is efficiently calculated in momentum space, and we use a cylindrical cut-off in order to negate the effects of aliasing from the Fourier transforms.

To derive the effective one-dimensional model, we follow ref. ⁴⁵ by assuming a wavefunction decomposition

$$\Psi(\overrightarrow{x},t) = \Phi(x,y,l,\eta)\psi(z,t) \equiv \frac{1}{\sqrt{\pi l}} e^{-(\eta x^2 + y^2/\eta)/2l^2} \psi(z,t),$$
 (2)

with variational parameters l and η representing the width of the radial wavefunction and the anisotropy of the state, respectively. Integrating out the transverse directions (x,y) in Eq. (1) upon substitution of the ansatz above gives the continuous quasi-one-dimensional eGPE, which when combined with a variational minimization of the energy functional to find (l,η) gives close agreement to the full 3D eGPE⁴⁵. We further decompose the longitudinal wave function $\psi(z,t)$ into a sum of Wannier functions w(z) of the lowest energy band over all lattice sites

$$\psi(z,t) = \sqrt{N} \sum_{i} c_{j}(t) w(z - z_{j}), \qquad (3)$$

for complex amplitudes c_j , and positions of lattice minima $z_j = (\lambda/2)j$. For deep enough lattices, the Wannier functions are well approximated by Gaussians of the form $w(z) = (\pi l_{\text{latt}}^2)^{-1/4} e^{-z^2/2l_{\text{bat}}^2}$, with $l_{\text{latt}} = (k\sqrt[4]{s})^{-1}$. After multiplying on the left by c_j^* and integrating over z, we obtain a set of discrete effective one-dimensional eGPEs

$$i\hbar\frac{\partial c_{j}}{\partial t} = -J(c_{j+1} + c_{j-1}) + \left(-F_{\rm ext}z_{j} + V_{\rm harm}(z) + g^{\rm 1D}N|c_{j}|^{2} + N\sum_{k}U^{\rm dd}_{|j-k|}|c_{k}|^{2} + \gamma^{\rm 1D}_{\rm QF}N^{3/2}\gamma_{\rm QF}|c_{j}|^{3}\right)c_{j}, \tag{4}$$

with the reduced effective one-dimensional parameters $\gamma_{\rm QF}^{\rm 1D} =$

 $2^{3/2}/(5\pi^{3/2}l^2l_{\rm latt})^{3/2}\gamma_{\rm QF}$ and $g^{\rm 1D}=g/((2\pi)^{3/2}l^2l_{\rm latt})$. Here, J denotes the tunneling rate between two neighboring lattice sites. The dipolar interaction coefficients between lattice sites j and k depend both on the separation |j-k|, and non-trivially on the size l and anisotropy η of the transverse cloud. For the variational minimization, we generate an interpolating function for a sensible range of (l,η) and separations up to |j-k|=6 via

$$U_{|j-k|}^{\mathrm{dd}}(l,\eta) = \int d^{3}\overrightarrow{x} \left\{ |\Psi_{0}(\overrightarrow{x} - z_{|j-k|}\hat{e}_{z}, l, \eta)|^{2} \right.$$

$$\times \int d^{3}\overrightarrow{x}' U_{\mathrm{dd}}(\overrightarrow{x} - \overrightarrow{x}') |\Psi_{0}(\overrightarrow{x}', l, \eta)|^{2} \right\}, \tag{5}$$

where $\Psi_0(\overrightarrow{x}',l,\eta) = \Phi(x,y,l,\eta)w(z)$ [see Eqs. (2) and (3)]. This allows us to simply look up the values of $U^{\mathrm{dd}}_{|j-k|}$ without having to recalculate for every time step during the energy minimization. We note that the energy contribution rapidly declines for separations larger than 2 sites, and find that 6 is more than sufficient to quantitatively describe the physics.

To find the stationary state solution of Eq. (4) (without gravity) we employ an imaginary time-evolution in combination with an optimization scheme, aiming to find the state which minimizes the total energy functional

$$\mathcal{E}[\mathbf{c};l,\eta] = \mathcal{E}_{\perp}[l,\eta] + \mathcal{E}_{\parallel}[\mathbf{c};l,\eta], \tag{6}$$

where $\mathbf{c} = (c_1, c_2, ..., c_n)$ for n total lattice sites. Here, $\mathcal{E}_{\perp}[l, \eta]$ gives the energy contribution from the transverse variational wave function, which reads

$$\mathcal{E}_{\perp}[l,\eta] = \frac{\hbar^2}{2ml^2} \left(\eta + \frac{1}{\eta} \right) + \frac{ml^2}{4} \left(\frac{\omega_x^2}{\eta} + \eta \omega_y^2 \right). \tag{7}$$

The latter term of Eq. (6) gives the discrete energy functional for the amplitudes c_p which includes the tunneling and all interaction terms

$$\mathcal{E}_{\parallel}[\mathbf{c}; l, \eta] = -\sum_{j} J(c_{j+1} + c_{j-1})c_{j}$$

$$+ \frac{1}{2} N \mathbf{g}^{1D} \sum_{j} |c_{j}|^{4} + \frac{1}{2} N \sum_{j,k} U_{|j-k|}^{dd} |c_{k}|^{2} |c_{j}|^{2}$$

$$+ \frac{2}{5} N^{3/2} \gamma_{\text{QF}}^{\text{1D}} \sum_{j} |c_{j}|^{5}.$$
(8)

Starting from an initial distribution of the amplitudes c_j we first determine the variational parameters (l,η) , which is done via an optimization scheme minimizing Eq. (8). Subsequently, we evolve the amplitudes in imaginary time using Eq. (4) and repeat this process until we find the minimum of the total energy function Eq. (6). Once we have the ground state of the system, we employ the discrete effective one-dimensional eGPE in real-time to simulate the Bloch oscillations in the presence of gravity. To account for changing transverse widths, after removing the harmonic potential from the optical dipole traps, we take l and η from the harmonic oscillator length calculated from the residual trapping potential of the lattice beams, given by $l = \sqrt{l_x l_y}$ and $\eta = l_y/l_x$. This provides a good approximation to the time averaged transverse behavior, which we have verified through comparison with the 3D eGPE.

Experimental protocol. We prepare a ^{166}Er spin-polarized BEC similar to ref. 4 . The magnetic field during the evaporation is along the z-axis with absolute value $|\mathbf{B}| = B_z = 1.9 \text{ G } (a_s = 80(1) \, a_0)$, see Fig. 1a. The magnetic field sets also the value of the scattering length thanks to a Feshbach resonance, centered close to 0 G. For the magnetic field range considered in this work, the \mathbf{B} -to- a_s conversion has been precisely mapped out in previous experiments 4,20 . Before loading the lattice, we rotate the magnetic field direction along the y-axis in 50 ms and change its absolute value to set the scattering length. At this step, we typically achieve 5×10^4 atoms with more than 60% condensed fraction in a cigar shape dipole trap with trapping frequencies $\omega_{x,y,z} = 2\pi \, (240(3), 30(3), 217(1))$ Hz. For our experiments, the atoms are then loaded in a 1D lattice by a 20 ms exponential ramp of the lattice depth. This is the experimental protocol used in Figs. 1, 2, and 3a.

To study the reversibility of the interaction-induced transition to a single lattice site (Fig. 3b), i.e., the evolution of the contrast due to a change of the scattering length, we employ a different protocol from the one above. In fact, in our experiment, the magnetic field along the y-direction can be changed on a timescale of \simeq 20 ms, which is slower compared to the z-direction (\simeq 1 ms). For this dataset, we prepare the BEC with $\mathbf{B} = (0, 0.25, 1) \mathrm{G}$ and then we load the lattice as described above. We then linearly ramp the field in 20 ms to $\mathbf{B} = (0, 0.25, 0) \mathrm{G}$ and record the

time evolution. In Fig. 3b, we study the contrast evolution after the ramp. For the black dataset, the magnetic field is quenched back to the initial value after 10 ms.

For Fig. 4, we extract the atom number condensed in the lattice by releasing the cloud from the combined ODT-lattice trap and by performing an absorption imaging after 30 ms of TOF. We integrate the density along the lattice axis and use a double Gaussian fit on the integrated density profile. We repeat the sequence 4–8 times for every scattering length. At low scattering lengths, we find a decreased number of condensed atoms, see Fig. 4. We attribute this to an increase of three-body loss in the vicinity of a Feshbach resonance⁴ and the increased density of the groundstate.

Contrast of the interference pattern. The density modulation that usually characterizes a BEC loaded into a 1D lattice can be experimentally extracted from the matter-wave interferometry after a TOF expansion 55 . To study the transition to one single occupied lattice site, we record the density distribution as a function of a_s . In more details, for each picture we perform a Fourier transform (FT) of the integrated momentum distribution, $n(q_z)$. In the contact dominated regime, the lattice induces two sidepeaks at $\pm q_z^*$ in $n(q_z)$. Consequently, in the FT analysis the peaks are at $z^* \simeq \lambda_{\text{lattice}}$. The visibility of the interference pattern is then estimated as $n_{\text{FT}}(|z^*|)/n_{\text{FT}}(0)$.

Data availability

Experimental data is available on reasonable request from the authors.

Code availability

Code used to generate the theory results is available on reasonable request from the authors.

Received: 16 May 2022; Accepted: 31 August 2022; Published online: 15 September 2022

References

- Tanzi, L. et al. Observation of a dipolar quantum gas with metastable supersolid properties. *Phys. Rev. Lett.* 122, 130405 (2019).
- Böttcher, F. et al. Transient supersolid properties in an array of dipolar quantum droplets. *Phys. Rev. X* 9, 011051 (2019).
- Chomaz, L. et al. Long-lived and transient supersolid behaviors in dipolar quantum gases. *Phys. Rev. X* 9, 021012 (2019).
- Chomaz, L. et al. Quantum-fluctuation-driven crossover from a dilute Bose-Einstein condensate to a macrodroplet in a dipolar quantum fluid. *Phys. Rev.* X 6, 041039 (2016).
- Schmitt, M., Wenzel, M., Böttcher, F., Ferrier-Barbut, I. & Pfau, T. Self-bound droplets of a dilute magnetic quantum liquid. *Nature* 539, 259–262 (2016).
- Norcia, M. A. & Ferlaino, F. Developments in atomic control using ultracold magnetic lanthanides. *Nat. Phys.* 17, 1349–1357 (2021).
- 7. Chomaz, L. et al. Dipolar physics: a review of experiments with magnetic quantum gases. Preprint at https://arxiv.org/abs/2201.02672 (2022).
- Cabrera, C. R. et al. Quantum liquid droplets in a mixture of Bose-Einstein condensates. Science 359, 301–304 (2018).
- Semeghini, G. et al. Self-bound quantum droplets of atomic mixtures in free space. Phys. Rev. Lett. 120, 235301 (2018).
- Petrov, D. S. Quantum mechanical stabilization of a collapsing Bose-Bose mixture. Phys. Rev. Lett. 115, 155302 (2015).
- Baillie, D., Wilson, R. M., Bisset, R. N. & Blakie, P. B. Self-bound dipolar droplet: a localized matter wave in free space. *Phys. Rev. A* 94, 021602 (2016).
- Lima, A. R. P. & Pelster, A. Quantum fluctuations in dipolar Bose gases. Phys. Rev. A 84, 041604 (2011).
- Cikojević, V., Markić, L. V., Astrakharchik, G. & Boronat, J. Universality in ultradilute liquid Bose-Bose mixtures. Phys. Rev. A 99, 023618 (2019).
- Ota, M. & Astrakharchik, G. Beyond lee-huang-yang description of self-bound Bose mixtures. SciPost Phys. 9, 20 (2020).
- Roati, G. et al. Atom interferometry with trapped fermi gases. *Phys. Rev. Lett.* 92, 230402 (2004).
- Ferrari, G., Poli, N., Sorrentino, F. & Tino, G. M. Long-lived bloch oscillations with bosonic sr atoms and application to gravity measurement at the micrometer scale. *Phys. Rev. Lett.* 97, 060402 (2006).
- Gustavsson, M. et al. Control of interaction-induced dephasing of bloch oscillations. Phys. Rev. Lett. 100, 080404 (2008).
- Fattori, M. et al. Magnetic dipolar interaction in a Bose-Einstein condensate atomic interferometer. Phys. Rev. Lett. 101, 190405 (2008).
- Baier, S. et al. Realization of a strongly interacting fermi gas of dipolar atoms. *Phys. Rev. Lett.* 121, 093602 (2018).

- Patscheider, A. et al. Determination of the scattering length of erbium atoms. *Phys. Rev. A* 105, 063307 (2022).
- Bloch, I., Dalibard, J. & Zwerger, W. Many-body physics with ultracold gases. Rev. Mod. Phys. 80, 885–964 (2008).
- Bloch, I., Dalibard, J. & Nascimbène, S. Quantum simulations with ultracold quantum gases. Nat. Phys. 8, 267 (2012).
- Gross, C. & Bloch, I. Quantum simulations with ultracold atoms in optical lattices. Science 357, 995–1001 (2017).
- Trefzger, C., Menotti, C., Capogrosso-Sansone, B. & Lewenstein, M. Ultracold dipolar gases in optical lattices. J. Phys. B: At. Mol. Optical Phys. 44, 193001 (2011).
- Dutta, O. et al. Non-standard hubbard models in optical lattices: a review. Rep. Prog. Phys. 78, 066001 (2015).
- Baier, S. et al. Extended Bose-Hubbard models with ultracold magnetic atoms. Science 352, 201–205 (2016).
- de Paz, A. et al. Nonequilibrium quantum magnetism in a dipolar lattice gas. Phys. Rev. Lett. 111, 185305 (2013).
- Lepoutre, S. et al. Out-of-equilibrium quantum magnetism and thermalization in a spin-3 many-body dipolar lattice system. Nat. Commun. 10, 1714 (2019).
- Gabardos, L. et al. Relaxation of the collective magnetization of a dense 3d array of interacting dipolar s = 3 atoms. *Phys. Rev. Lett.* 125, 143401 (2020).
- Patscheider, A. et al. Controlling dipolar exchange interactions in a dense three-dimensional array of large-spin fermions. *Phys. Rev. Res.* 2, 023050 (2020)
- Pasquiou, B. et al. Spin relaxation and band excitation of a dipolar Bose-Einstein condensate in 2d optical lattices. Phys. Rev. Lett. 106, 015301 (2011).
- Tang, Y. et al. Thermalization near integrability in a dipolar quantum newton's cradle. *Phys. Rev. X* 8, 021030 (2018).
- 33. Koch, T. et al. Stabilization of a purely dipolar quantum gas against collapse. *Nat. Phys.* 4, 218–222 (2008).
- Müller, S. et al. Stability of a dipolar Bose-Einstein condensate in a onedimensional lattice. Phys. Rev. A 84, 053601 (2011).
- Köberle, P. & Wunner, G. Phonon instability and self-organized structures in multilayer stacks of confined dipolar Bose-Einstein condensates in optical lattices. *Phys. Rev. A* 80, 063601 (2009).
- Klawunn, M. & Santos, L. Hybrid multisite excitations in dipolar condensates in optical lattices. *Phys. Rev. A* 80, 013611 (2009).
- Wilson, R. M. & Bohn, J. L. Emergent structure in a dipolar Bose gas in a onedimensional lattice. *Phys. Rev. A* 83, 023623 (2011).
- Rosenkranz, M., Cai, Y. & Bao, W. Effective dipole-dipole interactions in multilayered dipolar Bose-Einstein condensates. *Phys. Rev. A* 88, 013616 (2013).
- Wang, D.-W. Quantum phase transitions of polar molecules in bilayer systems. Phys. Rev. Lett. 98, 060403 (2007).
- Trefzger, C., Menotti, C. & Lewenstein, M. Pair-supersolid phase in a bilayer system of dipolar lattice bosons. *Phys. Rev. Lett.* 103, 035304 (2009).
- Macia, A., Astrakharchik, G. E., Mazzanti, F., Giorgini, S. & Boronat, J. Singleparticle versus pair superfluidity in a bilayer system of dipolar bosons. *Phys. Rev. A* 90, 043623 (2014).
- Gligorić, G., Maluckov, A., Hadžievski, Lcv & Malomed, B. A. Bright solitons in the one-dimensional discrete gross-pitaevskii equation with dipole-dipole interactions. *Phys. Rev. A* 78, 063615 (2008).
- Tikhonenkov, I, Malomed, B. A. & Vardi, A. Anisotropic solitons in dipolar Bose-Einstein condensates. *Phys. Rev. Lett.* 100, 090406 (2008).
- Raghunandan, M. et al. Two-dimensional bright solitons in dipolar Bose-Einstein condensates with tilted dipoles. Phys. Rev. A 92, 013637 (2015).
- Blakie, P. B., Baillie, D. & Pal, S. Variational theory for the ground state and collective excitations of an elongated dipolar condensate. *Commun. Theor. Phys.* 72, 085501 (2020).
- Blakie, P., Baillie, D., Chomaz, L. & Ferlaino, F. Supersolidity in an elongated dipolar condensate. *Phys. Rev. Res.* 2, 043318 (2020).
- Aikawa, K. et al. Bose-einstein condensation of erbium. Phys. Rev. Lett. 108, 210401 (2012).
- 48. Chin, C., Grimm, R., Julienne, P. S. & Tiesinga, E. Feshbach resonances in ultracold gases. *Rev. Mod. Phys.* 82, 1225–1286 (2010).
- Petrov, D. S. & Shlyapnikov, G. V. Interatomic collisions in a tightly confined Bose gas. *Phys. Rev. A* 64, 012706 (2001).
- Ben Dahan, M., Peik, E., Reichel, J., Castin, Y. & Salomon, C. Bloch oscillations of atoms in an optical potential. *Phys. Rev. Lett.* 76, 4508–4511 (1996)
- Fattori, M. et al. Atom interferometry with a weakly interacting Bose-Einstein condensate. *Phys. Rev. Lett.* 100, 080405 (2008).
- Fallani, L., Fort, C. & Inguscio, M. Bose-Einstein condensates in disordered potentials. In Advances in Atomic, Molecular, and Optical Physics, vol. 56, 119–160 (Academic Press, 2008).
- Morsch, O. & Oberthaler, M. Dynamics of Bose-Einstein condensates in optical lattices. Rev. Mod. Phys. 78, 179–215 (2006).

- Zin, P., Pylak, M., Wasak, T., Jachymski, K. & Idziaszek, Z. Quantum droplets in a dipolar Bose gas at a dimensional crossover. J. Phys. B At. Mol. Optical Phys. 54, 165302 (2021).
- Greiner, M., Mandel, O., Esslinger, T., Hänsch, T. W. & Bloch, I. Quantum phase transition from a superfluid to a mott insulator in a gas of ultracold atoms. *Nature*. 415, 39–44 (2002).
- Maluckov, A., Hadžievski, Lcv, Malomed, B. A. & Salasnich, L. Solitons in the discrete nonpolynomial schrödinger equation. *Phys. Rev. A* 78, 013616 (2008).
- Shabat, A. & Zakharov, V. Exact theory of two-dimensional self-focusing and one-dimensional self-modulation of waves in nonlinear media. Sov. Phys. IETP 34, 62 (1972).
- Pal, S., Baillie, D. & Blakie, P. Infinite dipolar droplet: A simple theory for the macrodroplet regime. *Phys. Rev. A* 105, 023308 (2022).
- Edmonds, M., Bland, T. & Parker, N. Quantum droplets of quasi-one-dimensional dipolar Bose–Einstein condensates. J. Phys. Comm. 4, 125008 (2020).
- Pedri, P. & Santos, L. Two-dimensional bright solitons in dipolar Bose-Einstein condensates. *Phys. Rev. Lett.* 95, 200404 (2005).
- Cheiney, P. et al. Bright soliton to quantum droplet transition in a mixture of Bose-Einstein condensates. *Phys. Rev. Lett.* 120, 135301 (2018).
- Drazin, P. G. & Johnson, R. Solitons: an introduction, vol. 2 (Cambridge University Press, 1989).
- Cuevas, J., Malomed, B. A., Kevrekidis, P. & Frantzeskakis, D. Solitons in quasi-one-dimensional Bose-Einstein condensates with competing dipolar and local interactions. *Phys. Rev. A* 79, 053608 (2009).
- Eichler, R., Zajec, D., Köberle, P., Main, J. & Wunner, G. Collisions of anisotropic two-dimensional bright solitons in dipolar Bose-Einstein condensates. *Phys. Rev. A* 86, 053611 (2012).
- Adhikari, S. K. Bright dipolar Bose-Einstein-condensate soliton mobile in a direction perpendicular to polarization. *Phys. Rev. A* 90, 055601 (2014).
- Baizakov, B., Al-Marzoug, S. & Bahlouli, H. Interaction of solitons in onedimensional dipolar Bose-Einstein condensates and formation of soliton molecules. *Phys. Rev. A* 92, 033605 (2015).
- Edmonds, M., Bland, T., Doran, R. & Parker, N. Engineering bright matterwave solitons of dipolar condensates. N. J. Phys. 19, 023019 (2017).
- Wächtler, F. & Santos, L. Quantum filaments in dipolar Bose-Einstein condensates. *Phys. Rev. A* 93, 061603 (2016).
- Bisset, R. N., Wilson, R. M., Baillie, D. & Blakie, P. B. Ground-state phase diagram of a dipolar condensate with quantum fluctuations. *Phys. Rev. A* 94, 033619 (2016).
- Ferrier-Barbut, I., Kadau, H., Schmitt, M., Wenzel, M. & Pfau, T. Observation of quantum droplets in a strongly dipolar Bose gas. *Phys. Rev. Lett.* 116, 215301 (2016).
- Lu, H.-Y. et al. Spatial density oscillations in trapped dipolar condensates. *Phys. Rev. A* 82, 023622 (2010).

Acknowledgements

We thank R.N. Bisset, A. Houwman, L. Lavoine, R. Grimm, and L. Tarruell for stimulating discussions, and B. Yang for his support in the early stage of the experiment. This work is financially supported through an ERC Consolidator Grant (RARE, no. 681432) and a DFG/FWF (FOR 2247/I4317-N36). We also acknowledge the Innsbruck Laser Core Facility, financed by the Austrian Federal Ministry of Science, Research and Economy. Part of the computational results presented have been achieved using the HPC infrastructure LEO of the University of Innsbruck.

Author contributions

G.N., D.S.G. and A.P. conducted the experiment and collected the experimental data. G.N. and L.L. analyzed the data. T.B., S.G., M.J.M and G.N. developed the theoretical model and performed the corresponding simulations. All the authors contributed to the writing of the paper. F.F. supervised the project.

Competing interests

The authors declare no competing interests.

Additional information

Supplementary information The online version contains supplementary material available at https://doi.org/10.1038/s42005-022-01009-8.

 $\textbf{Correspondence} \ \text{and} \ \text{requests for materials should be addressed to Francesca Ferlaino}.$

Peer review information *Communications Physics* thanks the anonymous reviewers for their contribution to the peer review of this work.

Reprints and permission information is available at http://www.nature.com/reprints

Publisher's note Springer Nature remains neutral with regard to jurisdictional claims in published maps and institutional affiliations.

Open Access This article is licensed under a Creative Commons Attribution 4.0 International License, which permits use, sharing, adaptation, distribution and reproduction in any medium or format, as long as you give appropriate credit to the original author(s) and the source, provide a link to the Creative Commons license, and indicate if changes were made. The images or other third party material in this article are included in the article's Creative Commons license, unless indicated otherwise in a credit line to the material. If material is not included in the article's Creative Commons license and your intended use is not permitted by statutory regulation or exceeds the permitted use, you will need to obtain permission directly from the copyright holder. To view a copy of this license, visit https://creativecommons.org/licenses/by/4.0/.

© The Author(s) 2022